

Earth and Space Science

RESEARCH ARTICLE

10.1029/2020EA001173

Key Points:

- Land cover transformation dominates wind speed and wind direction changes
- Land cover as well as soil texture transformations dominate temperature changes
- 3km resolution is optimal for wind condition simulation, however, 1km resolution favors temperature simulation

Supporting Information:

- Supporting Information

Correspondence to:

H. Qi,
hongqi@hit.edu.cn

Citation:

Fu, D., Liu, Y., Li, H., Liu, S., Li, B., Thapa, S., et al. (2020). Evaluating the impacts of land cover and soil texture changes on simulated surface wind and temperature. *Earth and Space Science*, 7, e2020EA001173. <https://doi.org/10.1029/2020EA001173>

Received 11 MAR 2020

Accepted 6 JUN 2020

Accepted article online 10 JUN 2020

Evaluating the Impacts of Land Cover and Soil Texture Changes on Simulated Surface Wind and Temperature

Donglei Fu¹ , Yuping Liu², Haizhi Li³, Songtao Liu⁴, Bo Li¹, Samit Thapa¹, Stephen Yabo¹, Xiazhong Sun¹, Bo Tang¹, Jinxiang Zuo¹, Hong Qi¹, and Chongguo Tian⁵ 

¹State Key Laboratory of Urban Water Resource and Environment, Harbin Institute of Technology, Harbin, China,

²Heilongjiang Provincial Environmental Science Research Institute, Harbin, China, ³Heilongjiang Provincial Environmental Monitoring Center Station, Harbin, China, ⁴Meteorological Observatory of Heilongjiang Province, Harbin, China, ⁵Key Laboratory of Coastal Environmental Processes and Ecological Remediation, Yantai Institute of Coastal Zone Research, Chinese Academy of Sciences, Yantai, China

Abstract In this study, Chinese Academy of Sciences land cover dataset (CAS_LC) and soil texture dataset (CAS_ST) as well as Tsinghua University land cover dataset (TU_LC) were incorporated into the Weather Research and Forecasting (WRF) model to evaluate the impacts of land cover and soil texture changes on the surface wind and air temperature as compared with outdated default datasets. Six modeling scenarios including single updating for the three new datasets, combined updating of new datasets (CAS_LC + CAS_ST, TU_LC + CAS_ST), and default datasets are designed. WRF simulations were conducted with three resolutions (9, 3, and 1 km) for the period of 14 July to 31 September 2017 over Harbin. Results of the 10-m wind speed, 10-m wind direction, and 2-m air temperature (T2) were evaluated against WRF default datasets (WLS). Results show that TU_LC-related simulations with lower mean absolute error (MAE) demonstrated the usefulness of this dataset in the wind speed simulation, while the changing soil texture exerted a limited effect on modeled wind. CAS_LC improved simulated wind direction and T2. Significant changes in the three variables were frequently induced by urban and built-up land or water bodies related transformations. The 3-km grid resolution was sufficient to reasonably simulate the surface winds and air temperature. The roughness length was a main factor disturbing the wind speed, while the land cover transformation was responsible for the changes in surface temperature and heat fluxes, thereby affecting T2 simulation.

1. Introduction

Geographical datasets affect land-atmosphere interface conditions by altering heat flux, hydrological cycle, and topographic relief, which are key factors influencing meteorological variables prescribed in models (Avissar & Schmidt, 1998; Chen & Dudhia, 2001; Ezber et al., 2007; LeMone et al., 2008; Pielke et al., 2011). Hence, adequately describing land surface features can ensure the precision of meteorological simulation by a weather forecasting model when combined with proper physical parametrization schemes (Lopez-Bravo et al., 2018). The Weather Research and Forecasting (WRF) model contains various static geographical datasets concerning land cover, topography, soil texture, and vegetation. However, they often are outdated and have a coarser resolution, which fails to depict land surface features due to dramatic disturbance caused by human activities (Boucher et al., 2004; Findell et al., 2007; Schubert & Grossman-Clarke, 2013). For example, the default 30-arc second USGS land cover dataset (hereafter referred to as USGS_LC) was updated in 1992, which underestimates urban and built-up land (hereafter referred to as UBL) proportion (Schicker et al., 2016) and leads to considerable misclassifications for the forest, cropland, and grassland in certain regions (Jimenez-Esteve et al., 2018; Thomas et al., 2018). In terms of the newest MODIS land cover dataset (hereafter referred to as MODIS_LC), underestimation for UBL and misrepresentation for forest are also existing on a large scale. Therefore, these outdated datasets are competent to investigate the changes in meteorological variables induced by land cover transformations.

The latest datasets presenting proper representation are crucial for conducting regional climate simulations. More attention has been paid to updated geographical datasets in recent years. These datasets include NLCD (land cover), GLCC (land cover), CORINE (land cover), SRTM (elevation), ASTER (elevation), and MODIS (land cover, vegetation, and snow cover). They have been introduced into the WRF model to investigate the

©2020 The Authors.

This is an open access article under the terms of the Creative Commons Attribution-NonCommercial License, which permits use, distribution and reproduction in any medium, provided the original work is properly cited and is not used for commercial purposes.

influences of changed land surface features on meteorological variables (Kumar et al., 2014; Li et al., 2017; Mallard et al., 2018; Santos-Alamillos et al., 2015). Some researchers incorporated localized geographical datasets obtained from various remote sensing images in WRF simulation (De Meij et al., 2015; Kurkowski et al., 2003; Li et al., 2018; Sertel et al., 2010). These studies have identified different effects from different physical schemes and discrepancies in geographical conditions adopted in modeling exercises (Lawston et al., 2015; Madala et al., 2019). Improvements were observed when different new geographical datasets were employed in simulations (Kirthinga & Patel, 2018). De Meij and Vinuesa (2014) introduced CORINE and STRM datasets in WRF and achieved good performance in the wind speed simulation in a summer period. Yang et al. (2018) obtained better predictions for the temperature and relative humidity while utilizing the latest land cover and leaf area index (LAI) datasets derived from MODIS. In the research conducted by He et al. (2017), improved elevation, land cover, vegetation fraction, and soil texture were simultaneously incorporated into the WRF, yielding remarkable improvements for the simulated air temperature and precipitation. It is worth noting that, these aforementioned studies were all focusing on those regions where dramatic changes in land surface features occurred.

In this work, extensive WRF simulations were conducted to investigate the surface meteorological conditions over Harbin, the biggest city located in northeastern China. Harbin was listed in The National Urban Agglomeration Project (NUAP) in 2013; since then, land cover had been strikingly altered by anthropogenic activities guided by agricultural regionalization and urban construction. As such, WRF default land cover and soil texture datasets failed to describe rapidly changed surface features. Hence, three new datasets, including the Chinese Academy of Sciences dataset for land cover (hereafter referred to as CAS_LC), soil texture dataset (hereafter referred to as CAS_ST), and Tsinghua University land cover dataset (hereafter referred to as TU_LC), were employed to investigate the effect of varied land surface parameters on meteorological variables. The key objectives are

1. to address the influences of land cover and soil texture on the modeled surface wind and temperature over Harbin and
2. to assess the advantages of the three new datasets in the WRF model.

2. Methods and Data

2.1. Study Area

Harbin (44.06–46.67 N, 125.70–130.17 E) is one of the representative traditional industrial cities in northeastern China. The city is located in southwest Heilongjiang province, with 11 million inhabitants and an area of 53,068 km². Harbin has a relatively low topographic complexity in elevation ranging from 81 to 1,643 m. Annual precipitation is 570 mm as the influence of a temperate continental monsoon climate and temperature varies from –28°C to 36°C.

2.2. New Datasets Information

The city experiences dramatic changes in its land cover induced by urbanization and agriculture and forest regionalization since the early 2000s. These land cover changes are so significant that the old USGS_LC and MODIS_LC are incapable of representing features of the land surface in reality. Specifically, USGS_LC and MODIS_LC substantially underestimate the UBL area, and noticeable disagreements of forest-related categories between these old datasets and realistic forest covers are also readily discerned. For soil texture, the default dataset with 30s resolution (hereafter referred to as DEFAULT_ST) manifests homogeneity by continuous and centralized distribution.

In the present study, two new land cover datasets and a soil texture dataset are employed. TU_LC dataset (Figure 1a) with a resolution of 30 m was developed by Tsinghua University based on Landsat and MOD13Q1 images in 2017, which reaches 72.35% precision on the global scale. The CAS_LC (Figure 1b) dataset with the 1-km resolution is based on Landsat8 OLI (2015) and GF-1 WFV images; this dataset is confined within China. CAS_ST (Figure 1e) with 1-km resolution is derived from <http://www.resdc.cn>. It consists of three categories of sand, silt, and clay. The detailed information for these datasets refers to Table S1.

In this study, the default USGS_LC and DEFAULT_ST were used as control simulation. USGS_LC is more suitable to investigate the impacts of land cover transformations on meteorological variables as compared

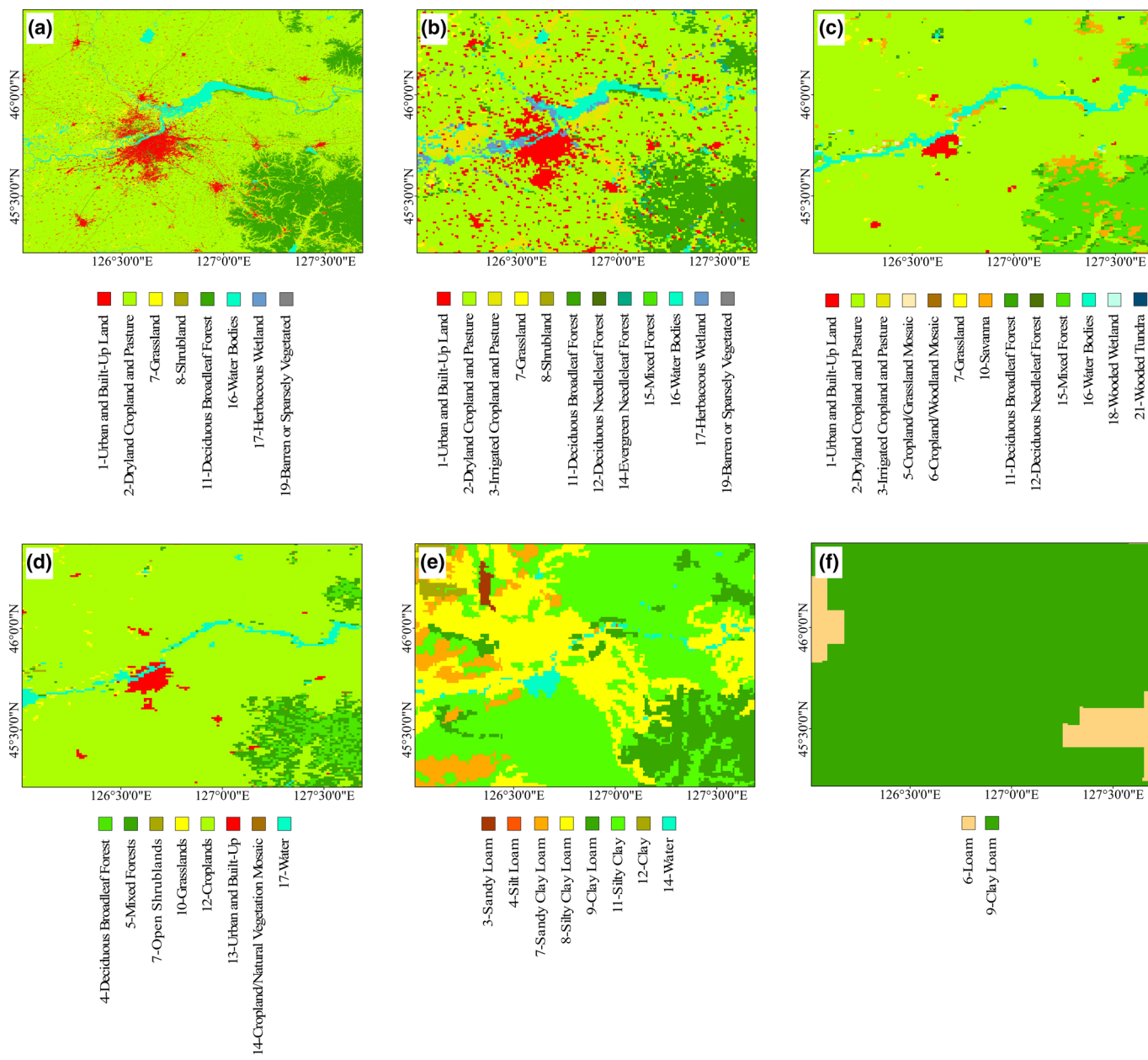


Figure 1. Land cover and soil texture datasets used in this study. (a) TU_LC, (b) CAS_LC, (c) USGS_LC, (d) MODIS_LC, (e) CAS_ST, (f) DEFAULT_ST.

with MODIS_LC because of abundant categories and higher heterogeneity (Figure 1c). Given differences in the classification system and data format between the default datasets and the three new datasets, the new datasets had been reprocessed to fit the model. Significant differences are found between the three new datasets and default datasets. For example, the UBL increases by 1,332 km² in CAS_LC as compared with that in USGS_LC, and the mixed forest defined in USGS_LC is basically transferred into deciduous broadleaf forest (hereafter referred to as DBF) by the new datasets. These obvious transformations provided an opportunity to investigate the effect of changed land surface parameters on meteorological variables in designated model sensitivity (scenario) runs.

2.3. WRF Configuration

WRF simulations over the period from 14 July to 31 September 2017 at a 3-hr interval were conducted using WRF version 3.9. The first 3 days were taken as spin-up time. Four nested domains with Lambert projection

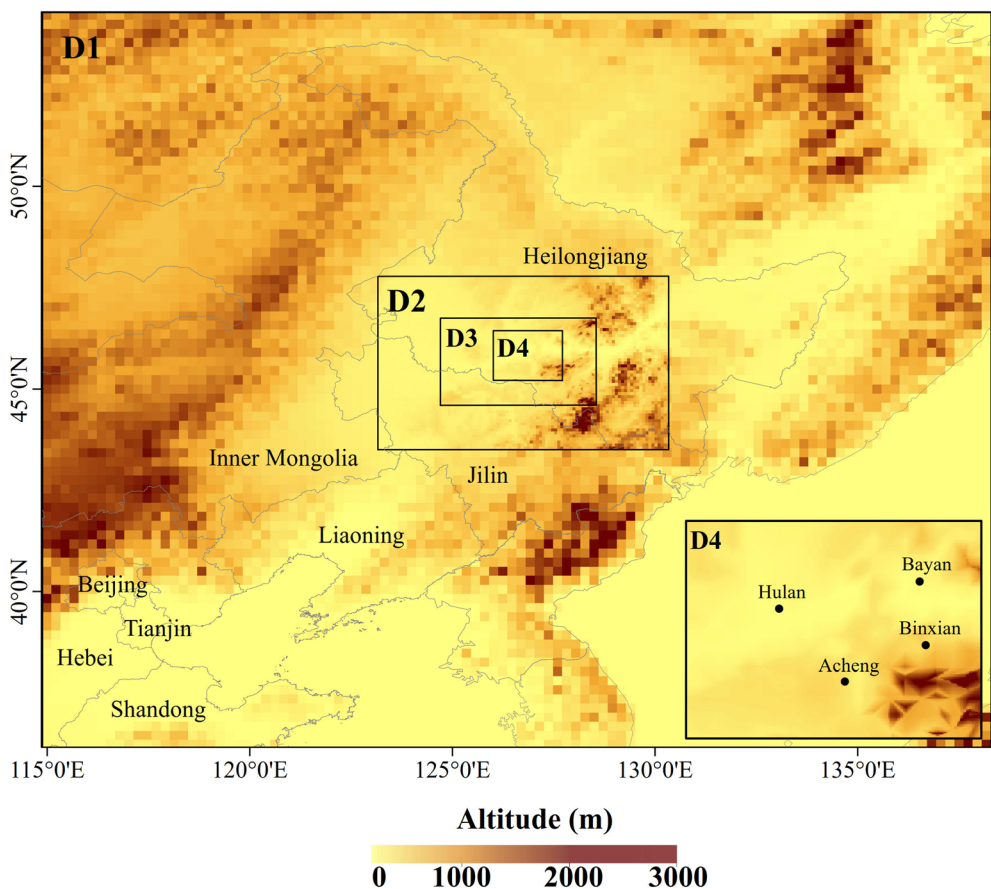


Figure 2. Domains used for this study with horizontal spatial resolutions of 27 (D1), 9 (D2), 3, (D3), and 1 km (D4). The solid circle in the right bottom inset denotes observational station. Altitude in shaded.

and horizontal resolutions ranging from 27 km (domain 1), 9 km (domain 2), 3 km (domain 3), to 1 km (domain 4) were adopted and defined as D1, D2, D3, and D4. A one-way interaction was used in the four domains. The main nest (D1) includes 83 by 74 grid points from east-west to north-south directions, covering the North China Plain, a small proportion of Inner Mongolia, and countries adjacent to Heilongjiang province. D2 is expended to the boundary of Harbin. The remaining two domains are located in Harbin's urban and suburban areas (Figure 2). In the vertical direction, 30 Eta levels in the range of 0–100 hPa are used. The 6-hr-interval FNL (Final Analysis) data with resolution 1° from the National Center for Environmental Prediction (NCEP) was selected as initial meteorological fields and lateral boundary conditions through interpolation. Modeled meteorology over D2, D3, and D4 domains was used for evaluating the sensitivity of variables to the grid resolutions. WRF has been widely used by Heilongjiang local meteorological department who provides helpful guidance for the model setup and physical parameterization schemes. Physical parameterizations adopted in present modeling investigations include (1) revised MM5 Monin-Obukhov scheme for surface layer (Jimenez et al., 2012), (2) the NOAH land surface scheme for land surface (Noah-LSM) (Chen & Dudhia, 2001), (3) Yonsei University Scheme for planetary boundary layer (Hong et al., 2006), (4) the Dudhia scheme for shortwave radiation (Dudhia, 1989), and (5) the RRTM scheme for longwave radiation (Mlawer et al., 1997).

Among these schemes, Noah-LSM should be specified for its impact on subgrid effect in land cover composition. In order to maintain the high resolution of the three new datasets to represent subgrid scale variability, the mosaic approach developed by Li et al. (2013) is adopted (Aas et al., 2017; Smirnova et al., 2016; Zhao & Wu, 2017). Here, in our study, the mean area fractions occupied by the sum of the three dominant tiles (with tile quantity option, in this study $N = 3$) are 98.8%, 97.2%, and 99.2% by TU_LC, CAS_LC, and USGS_LC, respectively. Because there exists only one urban category, the UCM scheme is abandoned.

Table 1
Model Simulation Scenarios

Simulation	Dataset	
	D1	D2, D3, D4
WLS	Default	Default
TL	Default	TU_LC
CL	Default	CAS_LC
TLCS	Default	TU_LC + CAS_ST
CLCS	Default	CAS_LC + CAS_ST
CS	Default	CAS_ST

Note. "Default" in the table contains USGS_LC and DEFAULT_ST.

2.4. Experimental Design and Model Evaluation

While an updated single land cover dataset was often examined for its sensitivity to modeling results, the new land cover and soil texture datasets were implemented simultaneously into WRF simulations. This was done because soil texture is a key driver for land cover variation (Whisler et al., 2016); also, Harbin is located in one of the world's three major black soil regions. The ability to conserve organic carbon makes black soil play a critical role in heat absorption, water allocation, and energy exchange. In terms of current soil properties, the area underwent severe tillage erosion (Zhao et al., 2018) and differs considerably from the original soil related dataset in WRF. Six model scenarios were designed to examine the sensitivities of the modeled surface winds and temperature to the changes in

land covers and soil textures (Table 1). For convenience, the WRF simulations by incorporating the three new datasets are hereafter referred to as "updated simulations."

In this study, the impacts of land cover and soil texture changes on the 10-m wind speed and direction, and 2-m air temperature (hereafter referred to as T2) are assessed. Observation data were provided by the China Meteorological Data Service Center (<http://www.nmic.cn/>) with 1-hr temporal resolution. Mean absolute error (MAE) is used to measure the differences between observation and simulation, BIAS is used to evaluate the model stability and whether the mode is the underpredictive or overpredictive (Bhimireddy & Bhaganagar, 2018), and the Pearson correlation coefficient (CC) is used to determine the strength of linear association between the simulation and observation.

Table 2

Average Mean Absolute Error (MAE) and the Pearson Correlation Coefficient (CC) of 2-m Air Temperature (°C) for Observational Stations with 9-, 3-, and 1-km Resolutions

	WLS_9km		CL_9km		CLCS_9km		TL_9km		TLCS_9km		CS_9km	
	MAE	CC	MAE	CC	MAE	CC	MAE	CC	MAE	CC	MAE	CC
Bayan	1.77	0.89	2.34	0.83	2.23	0.85	1.39	0.89	1.53	0.88	1.57	0.87
Hulan	1.91	0.88	1.63	0.88	1.58	0.87	1.42	0.88	1.46	0.89	1.57	0.88
Acheng	1.50	0.92	1.23	0.91	1.15	0.92	1.75	0.88	1.80	0.88	1.30	0.91
Binxian	2.12	0.82	1.84	0.82	1.67	0.83	2.30	0.80	2.19	0.81	2.06	0.82
Average	1.83	0.88	1.76	0.86	1.66	0.87	1.72	0.86	1.75	0.87	1.63	0.87
	WLS_3km		CL_3km		CLCS_3km		TL_3km		TLCS_3km		CS_3km	
	MAE	CC	MAE	CC	MAE	CC	MAE	CC	MAE	CC	MAE	CC
Bayan	1.71	0.90	1.44	0.87	1.56	0.88	1.47	0.88	1.61	0.88	1.72	0.85
Hulan	1.94	0.88	1.54	0.88	1.53	0.87	1.55	0.87	1.58	0.87	1.78	0.85
Acheng	1.54	0.92	1.78	0.88	1.77	0.89	1.84	0.88	1.83	0.88	1.39	0.89
Binxian	2.06	0.83	1.75	0.82	1.75	0.83	1.76	0.82	1.77	0.82	1.88	0.79
Average	1.81	0.88	1.63	0.86	1.65	0.87	1.66	0.86	1.70	0.86	1.69	0.85
	WLS_1km		CL_1km		CLCS_1km		TL_1km		TLCS_1km		CS_1km	
	MAE	CC	MAE	CC	MAE	CC	MAE	CC	MAE	CC	MAE	CC
Bayan	1.81	0.89	1.60	0.89	1.72	0.89	1.71	0.88	1.75	0.88	1.71	0.86
Hulan	1.88	0.87	1.63	0.88	1.53	0.88	1.55	0.87	1.61	0.87	1.69	0.85
Acheng	1.56	0.92	1.19	0.93	1.08	0.93	1.27	0.92	1.33	0.93	1.22	0.91
Binxian	2.07	0.82	1.86	0.82	1.71	0.83	1.84	0.82	1.81	0.82	1.84	0.79
Average	1.83	0.88	1.57	0.88	1.51	0.88	1.59	0.87	1.63	0.88	1.62	0.85

Note. WLS = simulation by using USGS_LC and DEFAULT_ST, CL = simulation by using CAS_LC, CLCS = simulation by using CAS_LC and CAS_ST, TL = simulation by using TU_LC, TLCS = simulation by using TU_LC and CAS_ST, CS = simulation by using CAS_ST. Bayan, Hulan, Acheng, and Binxian indicate the four observational stations.

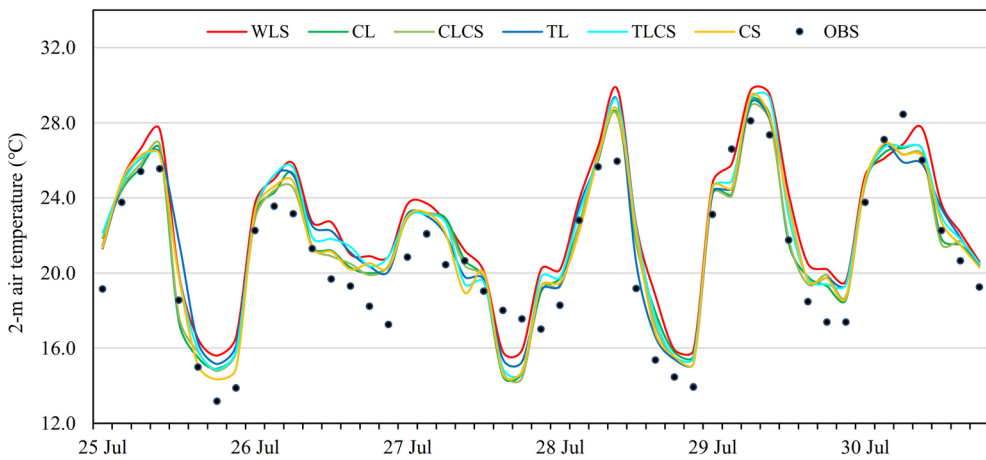


Figure 3. Time series of 3-hr intervals of simulated and observed 10-m wind speed with the 3-km resolution on 25 July to 30 July 2017. Results are averages over all observational stations for each period. Capital abbreviations are the same as Table 2. OBS = observational data.

$$MAE = \frac{1}{n} \sum_{i=1}^n |S_i - O_i|$$

$$BIAS = \frac{1}{n} \sum_{i=1}^n (S_i - O_i)$$

$$CC = \frac{\sum_{i=1}^n (S_i - S_a)(O_i - O_a)}{\sqrt{\sum_{i=1}^n (S_i - S_a)^2(O_i - O_a)^2}}$$

wherein S_i and O_i represent simulated and observed values, respectively, and S_a and O_a are their mean values. “ n ” is the total number of values.

3. Results

3.1. T2 Change

The impacts of new datasets on modeled mean T2 over the modeling period are shown in Table 2. Simulations with different resolutions are hereafter referred to as “simulation_resolution,” such as

Table 3
T2 Bias Resulting From Major Land Cover Transformations

USGS-CAS	Count	Percent (%)	T2BIAS (°C)	USGS-TU	Count	Percent (%)	T2BIAS (°C)
15-11	1,520	9.14	-0.23	15-11	1,351	8.12	-0.19
2-3	1,150	6.91	-0.35	2-1	818	4.91	-1.49
2-1	1,049	6.30	-1.73	2-7	630	3.79	-0.29
15-2	352	2.12	-0.01	2-11	262	1.58	-0.43
2-16	307	1.84	-0.88	15-2	216	1.30	0.03
2-11	271	1.63	-0.48	10-2	214	1.29	0.03
10-11	201	1.21	-0.23	2-16	195	1.17	-0.64
10-2	193	1.16	-0.06	10-11	180	1.08	-0.20
16-2	132	0.79	-0.14	16-2	141	0.85	0.01
11-2	105	0.63	0.05	11-2	110	0.66	0.12
2-17	92	0.55	-0.56	15-7	87	0.52	-0.01
16-3	67	0.40	-0.15	7-2	54	0.33	-0.11
2-7	59	0.35	-0.30	3-2	51	0.31	-0.19
7-2	55	0.33	-0.34	10-7	40	0.24	-0.03

Note. USGS-CAS/USGS-TU represents transformation occurred between USGS and CAS/TU, Count represents grid quantity for certain transformation, Percent represents grid quantity accounting for the total grid, and T2BIAS represents T2 bias. The number combination in the first column represents the number of land cover category which can refer to Figure 1.

Table 4
T2 Bias Resulting From Soil Texture Transformation

CS-DEFAULT	Count	Percent (%)	T2BIAS (°C)
Clay Loam-Silty clay	6,793	40.82	-0.26
Clay Loam-Silty Clay Loam	4,124	24.78	-0.24
Clay Loam-Sandy Clay Loam	996	5.99	-0.29
Loam-Clay Loam	584	3.51	-0.31
Loam-Silty Clay Loam	169	1.01	-0.42
Clay Loam-Clay	168	1.01	-0.39
Loam-Sandy Clay Loam	108	0.65	-0.46
Loam-Silty Clay	98	0.59	-0.34
Clay Loam-Sandy Loam	69	0.41	-0.25
Loam-Clay	30	0.18	-0.53
Clay Loam-Silt Loam	2	0.01	-0.24

Note. CS-DEFAULT represents transformation occurred between CS and default soil texture, Count represents grid quantity for certain transformation, Percent represents grid quantity accounting for the total grid, and T2BIAS represents T2 bias.

WLS_9km. The mean MAEs were improved by 0.11°C (9-km resolution), 0.15°C (3-km resolution), and 0.24°C (1-km resolution) by “updated simulations,” in contrast to WLS, where lower MAEs were found by CLCS and CL with 3- and 1-km resolution, indicating the better performance of CAS_LC with the two resolutions. Each simulation with different resolutions agreed well with observations, as shown in their respective CC values. Significant improvements by CLCS_3km were also observed in Hulan (-0.15°C), Acheng (-0.41°C), and Binxian (-0.31°C), whereas the improvement was very weak in Bayan station, indicating that these datasets are site-sensitive due to different UBL fractions within the same model grid.

Three-hour intervals of different scenarios with 3-km resolution from 25 July to 30 July 2017 are chosen to assess the performance of these new surface datasets (Figure 3). The model captured nicely the variation of the surface temperature. T2 was overestimated by all scenarios with different extents. Among them, the overestimation of T2 was more significant by WLS; this indicated the poor performance of WLS caused by lower precisions of default land cover and soil texture datasets. In the model, the 2-m air temperature is predicted by a surface energy balance equation which is primarily associated with radiation and sensible and latent heat fluxes, so T2 is strongly affected by the land cover transformation (Cao et al., 2018). Since such transformation could alter the surface albedo and energy balance, the increasing T2 could be ascribed to the transition from vegetated lands to urban lands, leading to the increasing heat island effect (Figure S1).

To further demonstrate the impacts of land cover changes on T2, a matrix table containing major land cover transformations by USGS versus CAS (hereafter referred to as USGS-CAS) and USGS versus TU (hereafter referred to as USGS-TU) is employed (Table 3). T2 cold bias dominated the matrix table by both USGS-CAS and USGS-TU, decreased by 0.39°C and 0.24°C on average, respectively. Among them, the conversion from mixed forest to DBF with the highest grid amount experienced mean temperature reduction at 0.21°C , which might be induced by certain differences of land surface parameters. A sharp decrease was subject to the switch from dryland cropland and pasture (hereafter referred to as DCP) to UBL, with an average of 1.61°C reduction. This was lower than an average decrease of 2.4°C by Yu et al. (2012) who incorporated the MODIS land cover dataset over the North China Plain to conduct a sensitive test. An average decrease of 0.45°C was observed when DCP-DBF occurred; the degree of reduction was higher than sensitive experiments reported by Shi et al. (2013) ($-0.4\text{--}0.0^{\circ}\text{C}$, northeast China) and Qu et al. (2013) (-0.13°C , the North China Plain) for the same transformation. All transferred soil categories experienced varying degrees of decrease (Table 4). The two dominated categories, conversions from clay loam to clay and clay loam to silty clay loam, yielded to the smallest decrease. The largest decrease occurred in the conversion from loam to clay.

3.2. Wind Speed

The lowest MAE for the 10-m wind speed occurred by TL and TLCS with the 3-km resolution, suggesting the advantage of TU_LC and the 3-km resolution in the WRF modeling of the wind speed, and further proved that the mosaic approach is less sensitive to high-resolution (Li et al., 2013). On the contrary, CS with

Table 5
Same as Table 2, But for 10-m Wind Speed With 3-km Resolution (m/s)

Station	MAE	CC	MAE	CC								
Bayan	1.24	0.37	1.2	0.36	1.12	0.39	1.14	0.37	1.12	0.56*	1.25	0.32
Hulan	0.88	0.28	0.94	0.23	0.95	0.2	0.65	0.21	0.64	0.3	1.45	0.23
Acheng	1.24	0.27	0.88	0.22	0.9	0.27	0.74	0.22	0.73	0.31	1.33	0.26
Binxian	1.5	0.32	1.41	0.35	1.36	0.41	1.18	0.43	1.14	0.38	1.36	0.29
Average	1.22	0.31	1.11	0.29	1.08	0.32	0.93	0.31	0.91	0.39	1.35	0.28

*Statistically significant level with $p < 0.05$.

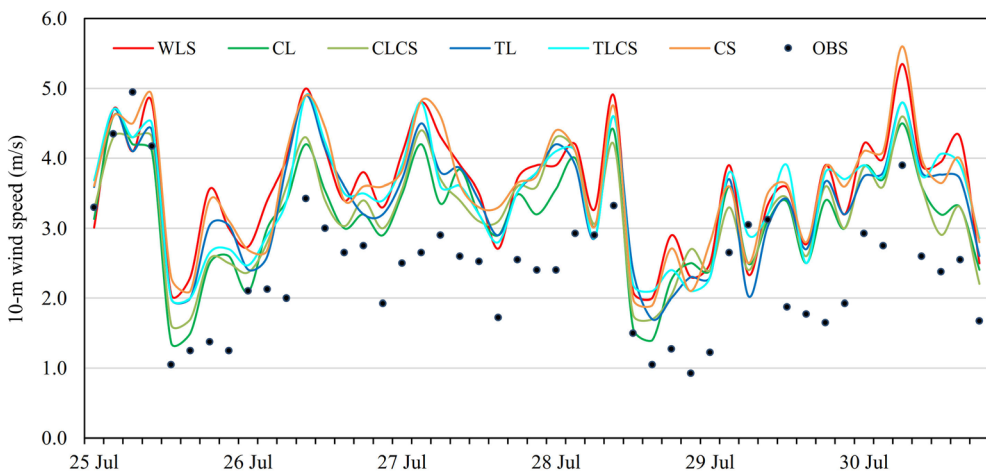


Figure 4. Same as Figure 3, but for 10-m wind speed.

3-km resolution performed poorly, manifesting that the land cover plays a dominant role in the wind speed simulation rather than soil texture (Table 5). The performances of the other two spatial resolutions are presented in Table S2. Changes in the wind speed averaged over all sampling sites subject to the 3-km resolution at intervals of 3-hr from 25 July to 30 July are displayed in Figure 4. All modeled wind speeds were overestimated against the measurements, but their variations approximately agreed with observations and also with previous studies (Madala et al., 2015; Zhang et al., 2013). The two new land cover datasets created new roughness lengths which markedly differed from the old datasets but featured more characteristics in the urban underlying surfaces. As such, stronger turbulences would be expected in the surface boundary layer (Jimenez et al., 2012).

The average BIAS from the major land cover transformations by USGS-CAS and USGS-TU were 0.06 and 0.04 m/s with the 3-km resolution, respectively (Table 6). Transformations featured by mixed forest and DCP were observed frequently. Conversion from mixed forest to DBF covered the highest number of grids at 1,520. DCP was generally converted into UBL over suburban areas. As a result, the wind speed approximately decreased by 0.33 and 0.35 m/s for USGS-CAS and USGS-TU over suburban areas, respectively. The result was similar to Li et al. (2018) for the same land transformation. Notable decreases for the wind speed were also observed in land to water transformations; for example, the conversion of DCP to water

Table 6
Same as Table 3, But for the 10-m Wind Speed

USGS-CAS	Count	Percent (%)	WSBIAS (m/s)	USGS-TU	Count	Percent (%)	WSBIAS (m/s)
15-11	1,520	9.14	-0.02	15-11	1,351	8.12	-0.03
2-3	1,150	6.91	-0.09	2-1	818	4.91	0.35
2-1	1,049	6.30	0.33	2-7	630	3.79	0.02
15-2	352	2.12	-0.25	2-11	262	1.58	0.27
2-16	307	1.84	-0.65	15-2	216	1.30	-0.22
2-11	271	1.63	0.23	10-2	214	1.29	0.04
10-11	201	1.21	0.23	2-16	195	1.17	-0.55
10-2	193	1.16	0.02	10-11	180	1.08	0.23
16-2	132	0.79	0.66	16-2	141	0.85	0.67
11-2	105	0.63	-0.24	11-2	110	0.66	-0.21
2-17	92	0.55	0.03	15-7	87	0.52	-0.23
16-3	67	0.40	0.51	7-2	54	0.33	0.05
2-7	59	0.35	-0.03	3-2	51	0.31	0.15
7-2	55	0.33	0.04	10-7	40	0.24	0.00

Table 7

Same as Table 2, But for 10-m Wind Direction with 3-km Resolution (°)

Station	MAE	CC										
Bayan	29.20	0.60*	23.52	0.59*	26.58	0.63*	27.89	0.56*	27.87	0.58*	27.73	0.62*
Hulan	47.76	0.46	38.48	0.48	42.89	0.48	44.59	0.49	47.52	0.44	45.18	0.47
Acheng	37.95	0.46	31.43	0.52	22.36	0.61	32.20	0.56	27.72	0.62	39.60	0.43
Binxian	54.33	0.34	46.53	0.37	49.94	0.34	47.82	0.41	54.36	0.31	51.98	0.35
Average	42.31	0.47*	34.99	0.49*	35.44	0.52	38.13	0.51	39.37	0.49	41.12	0.47

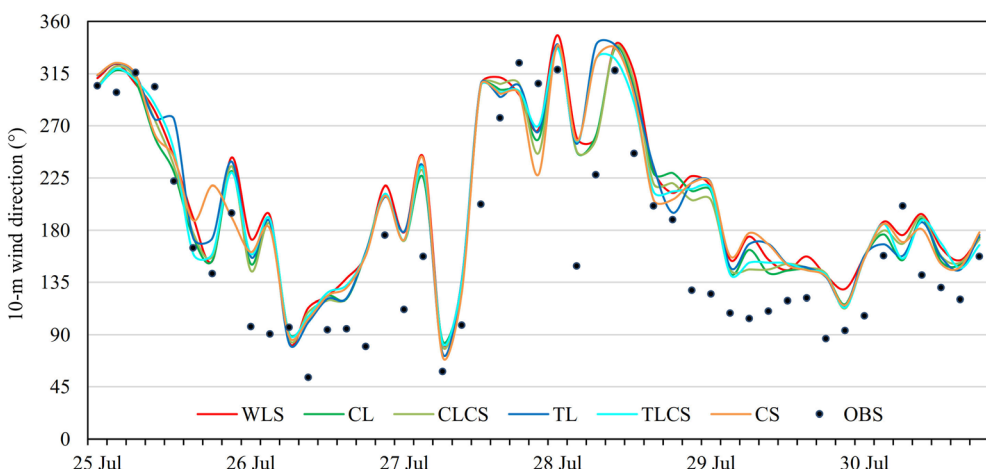
*Statistically significant level with $p < 0.05$.

bodies yielded a 0.65 m/s reduction. The magnitude of change in the wind speed was higher than a sensitive experiment by Qu et al. (2013) (with a decrease of 0.04 m/s), which might be ascribed to the use of the mosaic approach in this study. Soil texture change showed an averaged of -0.04 m/s decrease, with the maximum decrease of 0.13 m/s occurred by conversion from loam to silty clay loam, and thus generally exerted a limited effect on the wind speed variation (Table S3).

3.3. Wind Direction

Again, the 3-km resolution yielded the best prediction of the wind directions, as shown by lower MAE and the good agreement with observations. The best performance of CL suggests that CAS_LC is a very useful dataset in the wind direction simulations. On the other hand, limited improvements were observed by CS (Table 7). The performances of 9-km and 1-km spatial resolutions are presented in Table S4. Details for a typical period of different scenarios with the 3-km resolution are shown in Figure 5. As seen, CL illustrated the best improvement against observations. The causes of this improvement might be attributed to the more precise surface roughness length and better prediction of turbulence intensity, which had been proved by Wen et al. (2014).

Wind frequency from observation and simulation with the 3-km resolution is shown in Figure 6. Results were represented as the average of the four sampling stations throughout the simulation period. The other two spatial resolutions yielded similar wind frequency to the 3-km resolution. As shown in Figure 6, the southerly and northwesterly sectors showed larger proportions, accounting for 31–37% of all wind directions, matching well with the observation. However, there were large discrepancies between observations and simulations in the northwesterly and westerly wind sectors.

**Figure 5.** Same as Figure 3, but for the 10-m wind direction.

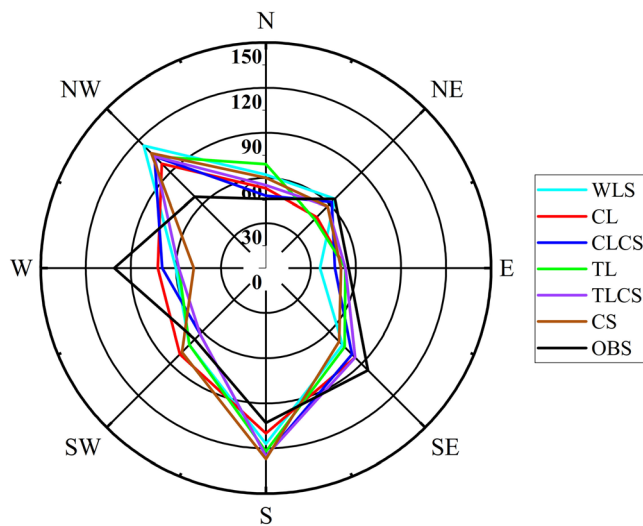


Figure 6. Wind frequency over simulation and observation with the 3-km resolution for all the 599 periods. The values in the circle indicate frequency. Capital abbreviations are the same as Table 2. OBS = observational data. Results are averaged over four observational stations for each scenario.

4. Discussions

4.1. Impacts of Land Cover Change on Wind Speed

The results of this study showed that land cover change played an important role in the modeled wind speed. Redundancy analysis was conducted by the wind speeds from TL simulation minus that from WLS scenario

over the urban and suburban regions of Harbin to investigate the influence of land surface parameters on the changes in the 10-m wind speed. The results are shown in Figure 7. In the figure, the black circle, the blue line with an arrow, and the red line with an arrow denote land cover transformations (the number of the land cover category is marked in Figure 1; for example, 11-15 means the conversion from mixed forest to DBF), the 10-m wind speed differences, and the differences of land surface parameters, respectively. These transformations which exhibited large wind speed reduction were positively correlated with the increase of ZOMAX (maximum background roughness length). Those bins with the wind increases primarily referred to water to land transformations, in which 16-7 and 16-2 exhibited larger abundance, and the increased wind speed had a close relationship with ZOMIN (minimum background roughness length).

Transformations were frequently found between TU_LC and USGS_LC, and 10-m wind speed was closely associated with the surface roughness length as mentioned above. Therefore, the influence of land cover changes induced roughness length on the 10-m wind speed over the urban and suburban regions by TL minus WLS was further elucidated (Figure 8). The variations of roughness length (Figure 8b) were always spatially corresponded to the changes in the 10-m wind speed. Three typical areas were used to examine the associations between land cover changes and wind speeds (Figure 8a). Area-1 was located in central urban and suburban areas of Harbin. The suburban area experienced considerable land cover changes, especially the transformation from UBL (TU_LC) to DCP (USGS_LC), over which the reduction of wind speed ranged from 0.3 to 0.9 m/s. The magnitude of the wind speed changes was higher than the result of Lai et al. (2016), in which the

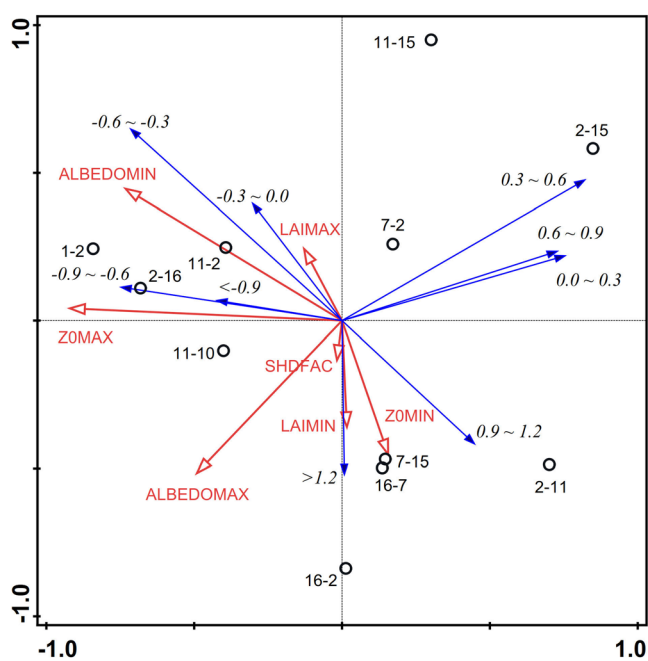


Figure 7. Redundancy analysis for influences of land cover changes on 10-m wind speed over D3 by TL minus WLS. The empty black circle indicates land cover change, label beside it, 11-15 for instance, represents category belonged to TU_LC (former) and USGS_LC (later) shown in Figure 1. The blue line with the arrow indicates a bin of wind speed difference (m/s). The red line with the arrow indicates vegetation parameter difference calculated by the corresponding land cover category.

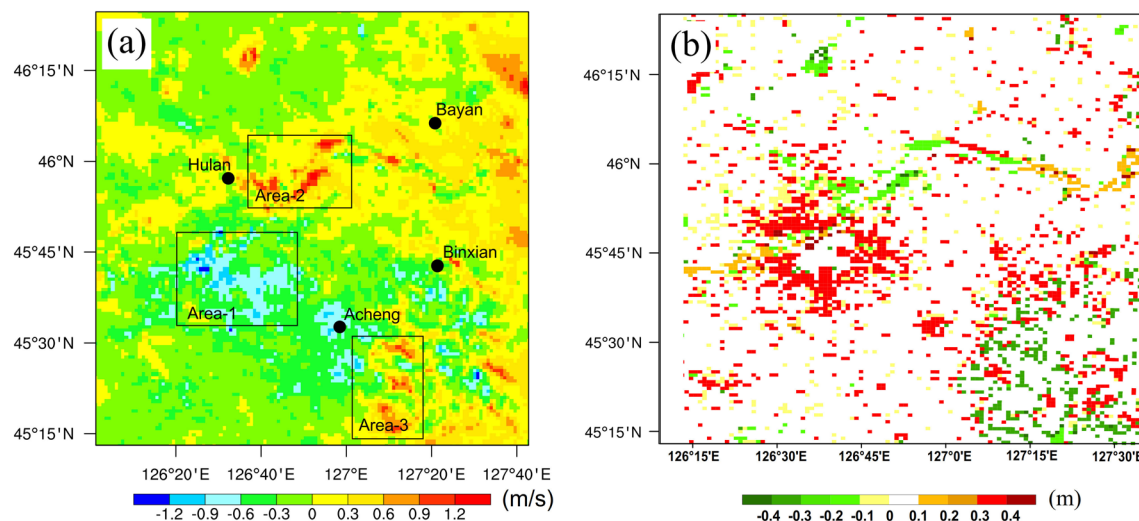


Figure 8. The differences in wind speed (a) and roughness length (b) by TL minus WLS over the urban and suburban regions of Harbin. Results are average for all the simulated periods. Solid circle for the observational station, rectangle for area influenced by land cover change.

10-m wind speed over the Pearl River Delta region decreased by 0.16 m/s in a summer month induced by varied surface parameters. Conversion from DCP to water bodies was identified in Area-2 where the decreasing roughness length increased the wind speed. The changes in the wind speed in Area-3 mainly were attributed to the dominant transformations from DBF or DCP to mixed forest, agreeing with the result by Sertel et al. (2011).

4.2. The Impacts of Land Cover Change on Wind Direction

The sensitivity of the wind directions to the changes in land cover is illustrated by the differences of the mean wind directions obtained from CL minus that from WLS with 3-km resolution (Figure 9). Wind direction varied intensely in the northeast of the model domain, because the land cover change from DCP to mixed forest was widely scattered in this area, particularly at those grids with a wind direction differences of 20° to 30°.

Wind directions at Hulan, Bayan, and Binxian station showed lower bias (<5°). The mosaic approach contributed to lower bias; in specific, wind direction was calculated separately based on land cover patches and

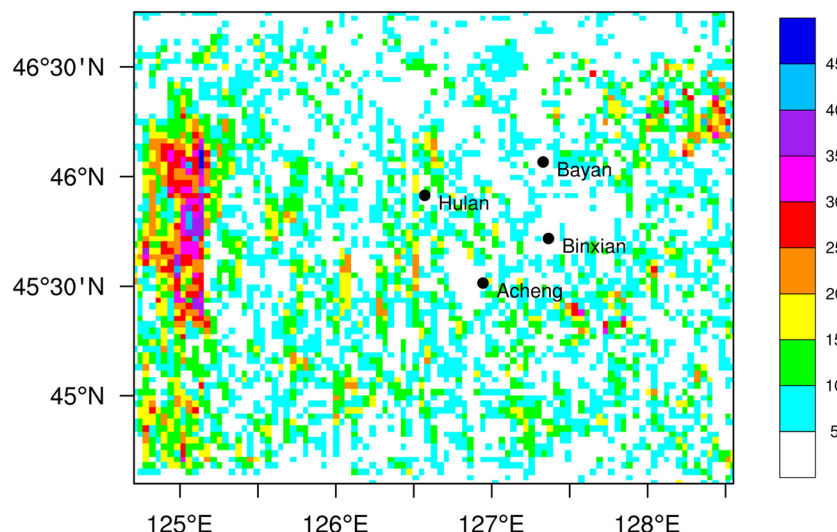


Figure 9. Absolute differences between CL and WLS for 10-m wind direction over D3. Results are average for all the periods. Solid circle for the observational station, the color scale at right for ranges of wind direction differences (°).

then averaged. The greatest variation occurred at Acheng station. This was likely because the station was surrounded by UBL in CAS_LC, whereas USGS_LC indicated a single DCP, resulting in the change in the surface roughness length. Santos-Alamillos et al. (2015) implemented a new land cover dataset to simulate the winds by WRF. Their results indicated that Málaga station showed larger wind direction discrepancies due to land cover misrepresentation, in line with our result in this study.

5. Conclusions

In this study, datasets incorporation is implemented by using CAS_LC, TU_LC, and CAS_ST to exploit the effects of land cover and soil texture changes on surface wind conditions and T2 over Harbin. Also, the optimal resolution coupled with the mosaic approach to fit the three datasets is confirmed. The main conclusions are summarized below.

Land cover transformation could mainly cause wind condition variation, in particular, along with those transformations related to UBL and water bodies, because the two categories exhibited distinct roughness lengths. Land cover transformations also contributed to the changes in T2, which could be attributed to the changes in radiation and surface energy balance. TU_LC was demonstrated to be useful for the 10-m wind speed simulation because TL and TLCS yielded lower MAE, while CL and CLCS achieved better improvement for the simulation of the 10-m wind direction. Results revealed that the coupling of the three updated datasets and a fine resolution domain, namely, the 3-km resolution mapping in this study, could yield significant improvements in the simulated 10-m winds and T2.

Data Availability Statement

The land cover dataset developed by Tsinghua University and soil texture production were downloaded from <http://www.geodata.cn/data/datadetails.html?dataguid=25725976218589> and <http://www.resdc.cn>. Detailed information for the WRF model can be referred from the WRFUsersGuide Version 3.9 (https://www2.mmm.ucar.edu/wrf/users/docs/user_guide_V3/contents.html). We thank the Global Data Assimilation System (GDAS) for providing FNL forcing data that can be downloaded from <https://rda.ucar.edu/datasets/ds083.2/index.html#sf01-wl-/data/ds083.2?g=2>. The observational data were derived from http://www.nmic.cn/dataService/cdcindex/datacode/A.0012.0001/show_value/normal.html. We state that samples of methods for data processing, NCL scripts for plotting, and the processed data (including shapefile, raster, NETCDF, etc.) are accessible to Mendeley Data Repository <https://data.mendeley.com/datasets/k7t3mrcm68/draft?a=a1b1ff94-bb46-407d-905f-2fefb8e7ce6f>.

Acknowledgments

We thank the National Science and Technology Infrastructure of China, as well as Data Center for Resources and Environmental Sciences belonged to the Chinese Academy of Sciences for their data service. This research was funded under the auspices of the National Key R&D Program of China (No. 2017YFC0212305) and the Open Project of State Key Laboratory of Urban Water Resource and Environment, Harbin Institute of Technology (No. HC201811). The authors also would like to thank the anonymous reviewers for constructive comments.

References

- Aas, K. S., Gisnas, K., Westermann, S., & Berntsen, T. K. (2017). A tiling approach to represent subgrid snow variability in coupled land surface-atmosphere models. *Journal of Hydrometeorology*, 18(1), 49–63. <https://doi.org/10.1175/jhm-d-16-0026.1>
- Avissar, R., & Schmidt, T. (1998). An evaluation of the scale at which ground-surface heat flux patchiness affects the convective boundary layer using large-eddy simulations. *Journal of the Atmospheric Sciences*, 55(16), 2666–2689. [https://doi.org/10.1175/1520-0469\(1998\)055<2666:Aeotsa>2.0.Co;2](https://doi.org/10.1175/1520-0469(1998)055<2666:Aeotsa>2.0.Co;2)
- Bhimireddy, S. R., & Bhaganagar, K. (2018). Short-term passive tracer plume dispersion in convective boundary layer using a high-resolution WRF-ARW model. *Atmospheric Pollution Research*, 9(5), 901–911. <https://doi.org/10.1016/j.apr.2018.02.010>
- Boucher, O., Myhre, G., & Myhre, A. (2004). Direct human influence of irrigation on atmospheric water vapour and climate. *Climate Dynamics*, 22(6–7), 597–603. <https://doi.org/10.1007/s00382-004-0402-4>
- Cao, Q., Yu, D. Y., Georgescu, M., & Wu, J. G. (2018). Substantial impacts of landscape changes on summer climate with major regional differences: The case of China. *Science of the Total Environment*, 625, 416–427. <https://doi.org/10.1016/j.scitotenv.2017.12.290>
- Chen, F., & Dudhia, J. (2001). Coupling an advanced land surface-hydrology model with the Penn State-NCAR MM5 modeling system. Part I: Model implementation and sensitivity. *Monthly Weather Review*, 129(4), 569–585. [https://doi.org/10.1175/1520-0493\(2001\)129<0569:Caaalsh>2.0.Co;2](https://doi.org/10.1175/1520-0493(2001)129<0569:Caaalsh>2.0.Co;2)
- De Meij, A., Bossioli, E., Penard, C., Vinuesa, J. F., & Price, I. (2015). The effect of SRTM and Corine Land Cover data on calculated gas and PM10 concentrations in WRF-Chem. *Atmospheric Environment*, 101, 177–193. <https://doi.org/10.1016/j.atmosenv.2014.11.033>
- De Meij, A., & Vinuesa, J. F. (2014). Impact of SRTM and Corine Land Cover data on meteorological parameters using WRF. *Atmospheric Research*, 143, 351–370. <https://doi.org/10.1016/j.atmosres.2014.03.004>
- Dudhia, J. (1989). Numerical study of convection observed during the winter monsoon experiment using a mesoscale two-dimensional model. *Journal of the Atmospheric Sciences*, 46(20), 3077–3107. [https://doi.org/10.1175/1520-0469\(1989\)046<3077:Nsocod>2.0.Co;2](https://doi.org/10.1175/1520-0469(1989)046<3077:Nsocod>2.0.Co;2)
- Ezber, Y., Sen, O. L., Kindap, T., & Karaca, M. (2007). Climatic effects of urbanization in Istanbul: A statistical and modeling analysis. *International Journal of Climatology*, 27(5), 667–679. <https://doi.org/10.1002/joc.1420>
- Findell, K. L., Sheviakova, E., Milly, P. C. D., & Stouffer, R. J. (2007). Modeled impact of anthropogenic land cover change on climate. *Journal of Climate*, 20(14), 3621–3634. <https://doi.org/10.1175/jcli4185.1>

- He, J. J., Yu, Y., Yu, L. J., Liu, N., & Zhao, S. P. (2017). Impacts of uncertainty in land surface information on simulated surface temperature and precipitation over China. *International Journal of Climatology*, 37(S1), 829–847. <https://doi.org/10.1002/joc.5041>
- Hong, S. Y., Noh, Y., & Dudhia, J. (2006). A new vertical diffusion package with an explicit treatment of entrainment processes. *Monthly Weather Review*, 134(9), 2318–2341. <https://doi.org/10.1175/mwr3199.1>
- Jimenez, P. A., Dudhia, J., Gonzalez-Rouco, J. F., Navarro, J., Montavez, J. P., & Garcia-Bustamante, E. (2012). A revised scheme for the WRF surface layer formulation. *Monthly Weather Review*, 140(3), 898–918. <https://doi.org/10.1175/mwr-d-11-00056.1>
- Jimenez-Esteve, B., Udina, M., Soler, M. R., Pepin, N., & Miro, J. R. (2018). Land use and topography influence in a complex terrain area: A high resolution mesoscale modelling study over the Eastern Pyrenees using the WRF model. *Atmospheric Research*, 202, 49–62. <https://doi.org/10.1016/j.atmosres.2017.11.012>
- Kirthiga, S. M., & Patel, N. R. (2018). Impact of updating land surface data on micrometeorological weather simulations from the WRF model. *Atmosfera*, 31(2), 165–183. <https://doi.org/10.20937/atm.2018.31.02.05>
- Kumar, A., Chen, F., Barlage, M., Ek, M. B., & Niyogi, D. (2014). Assessing impacts of integrating MODIS vegetation data in the weather research and forecasting (WRF) model coupled to two different canopy-resistance approaches. *Journal of Applied Meteorology and Climatology*, 53(6), 1362–1380. <https://doi.org/10.1175/jamc-d-13-0247.1>
- Kurkowski, N. P., Stensrud, D. J., & Baldwin, M. E. (2003). Assessment of implementing satellite-derived land cover data in the Eta model. *Weather and Forecasting*, 18(3), 404–416. [https://doi.org/10.1175/1520-0434\(2003\)18<404:Aoisd>2.0.Co;2](https://doi.org/10.1175/1520-0434(2003)18<404:Aoisd>2.0.Co;2)
- Lai, A. Q., Liu, Y. M., Chen, X. Y., Chang, M., Fan, Q., Chan, P. K., et al. (2016). Impact of land-use change on atmospheric environment using refined land surface properties in the Pearl River Delta, China. *Advances in Meteorology*, 2016(6), 1–15. <https://doi.org/10.1155/2016/3830592>
- Lawston, P. M., Santanello, J. A., Zaitchik, B. F., & Rodell, M. (2015). Impact of irrigation methods on land surface model spinup and initialization of WRF forecasts. *Journal of Hydrometeorology*, 16(3), 1135–1154. <https://doi.org/10.1175/jhm-d-14-0203.1>
- LeMone, M. A., Tewari, M., Chen, F., Alfieri, J. G., & Niyogi, D. (2008). Evaluation of the Noah land surface model using data from a fair-weather IHOP_2002 day with heterogeneous surface fluxes. *Monthly Weather Review*, 136(12), 4915–4941. <https://doi.org/10.1175/2008mwr2354.1>
- Li, D., Bou-Zeid, E., Barlage, M., Chen, F., & Smith, J. A. (2013). Development and evaluation of a mosaic approach in the WRF-Noah framework. *Journal of Geophysical Research: Atmospheres*, 118, 11,918–11,935. <https://doi.org/10.1002/2013JD020657>
- Li, J. Y., Zheng, X. Q., Zhang, C. X., & Chen, Y. M. (2018). Impact of land-use and land-cover change on meteorology in the Beijing-Tianjin-Hebei region from 1990 to 2010. *Sustainability*, 10(2), 176. <https://doi.org/10.3390/su10010176>
- Li, M. M., Wang, T. J., Xie, M., Zhuang, B. L., Li, S., Han, Y., et al. (2017). Improved meteorology and ozone air quality simulations using MODIS land surface parameters in the Yangtze River Delta urban cluster, China. *Journal of Geophysical Research: Atmospheres*, 122, 3116–3140. <https://doi.org/10.1002/2016JD026182>
- Lopez-Bravo, C., Caetano, E., & Magana, V. (2018). Forecasting summertime surface temperature and precipitation in the Mexico City metropolitan area: Sensitivity of the WRF model to land cover changes. *Frontiers in Earth Science*, 6, 1–14. <https://doi.org/10.3389/feart.2018.00006>
- Madala, S., Salinas, S. V., Wang, J., & Liew, S. C. (2019). Customization of the advanced research weather research and forecasting model over the Singapore region: Impact of planetary boundary layer schemes, land use, land cover and model horizontal grid resolution. *Meteorological Applications*, 26(2), 221–231. <https://doi.org/10.1002/met.1755>
- Madala, S., Satyanarayana, A. N. V., Srinivas, C. V., & Kumar, M. (2015). Mesoscale atmospheric flow-field simulations for air quality modeling over complex terrain region of Ranchi in eastern India using WRF. *Atmospheric Environment*, 107, 315–328. <https://doi.org/10.1016/j.atmosenv.2015.02.059>
- Mallard, M. S., Spero, T. L., & Taylor, S. M. (2018). Examining WRF's sensitivity to contemporary land use datasets across the contiguous United States using dynamical downscaling. *Journal of Applied Meteorology and Climatology*, 57(11), 2561–2583. <https://doi.org/10.1175/jamc-d-17-0328.1>
- Mlawer, E. J., Taubman, S. J., Brown, P. D., Iacono, M. J., & Clough, S. A. (1997). Radiative transfer for inhomogeneous atmospheres: RRTM, a validated correlated-k model for the longwave. *Journal of Geophysical Research*, 102, 16,663–16,682. <https://doi.org/10.1029/97JD00237>
- Pielke, R. A., Pitman, A., Niyogi, D., Mahmood, R., McAlpine, C., Hossain, F., et al. (2011). Land use/land cover changes and climate: Modeling analysis and observational evidence. *Wiley Interdisciplinary Reviews-Climate Change*, 2(6), 828–850. <https://doi.org/10.1002/wcc.144>
- Qu, R. J., Cui, X. L., Yan, H. M., Ma, E. J., & Zhan, J. Y. (2013). Impacts of land cover change on the near-surface temperature in the North China Plain. *Advances in Meteorology*, 2013, 1–12. <https://doi.org/10.1155/2013/409302>
- Santos-Alamillos, F. J., Pozo-Vazquez, D., Ruiz-Arias, J. A., & Tovar-Pescador, J. (2015). Influence of land-use misrepresentation on the accuracy of WRF wind estimates: Evaluation of GLCC and CORINE land-use maps in southern Spain. *Atmospheric Research*, 157, 17–28. <https://doi.org/10.1016/j.atmosres.2015.01.006>
- Schicker, I., Arias, D. A., & Seibert, P. (2016). Influences of updated land-use datasets on WRF simulations for two Austrian regions. *Meteorology and Atmospheric Physics*, 128(3), 279–301. <https://doi.org/10.1007/s00703-015-0416-y>
- Schubert, S., & Grossman-Clarke, S. (2013). The influence of green areas and roof albedos on air temperatures during extreme heat events in Berlin, Germany. *Meteorologische Zeitschrift*, 22(2), 131–143. <https://doi.org/10.1127/0941-2948/2013/0393>
- Sertel, E., Ormeci, C., & Robock, A. (2011). Modelling land cover change impact on the summer climate of the Marmara region, Turkey. *International Journal of Global Warming*, 3(1/2), 194–202. <https://doi.org/10.1504/ijgw.2011.038379>
- Sertel, E., Robock, A., & Ormeci, C. (2010). Impacts of land cover data quality on regional climate simulations. *International Journal of Climatology*, 30(13), 1942–1953. <https://doi.org/10.1002/joc.2036>
- Shi, Q. L., Lin, Y. Z., Zhang, E. P., Yan, H. M., & Zhan, J. Y. (2013). Impacts of cultivated land reclamation on the climate and grain production in Northeast China in the future 30 years. *Advances in meteorology*, 2013. <https://doi.org/10.1155/2013/853098>
- Smirnova, T. G., Brown, J. M., Benjamin, S. G., & Kenyon, J. S. (2016). Modifications to the rapid update cycle land surface model (RUC LSM) available in the weather research and forecasting (WRF) model. *Monthly Weather Review*, 144(5), 1851–1865. <https://doi.org/10.1175/mwr-d-15-0198.1>
- Thomas, L., Dash, S. K., Mohanty, U. C., & Babu, C. A. (2018). Features of western disturbances simulated over North India using different land-use data sets. *Meteorological Applications*, 25(2), 246–253. <https://doi.org/10.1002/met.1687>
- Wen, X. H., Liao, X. H., Yuan, W. P., Yan, X. D., Wei, Z. G., Liu, H. Z., et al. (2014). Numerical simulation and data assimilation of the water-energy cycle over semiarid northeastern China. *Science China-Earth Sciences*, 57(10), 2340–2356. <https://doi.org/10.1007/s11430-014-4914-4>

- Whisler, K. M., Rowe, H. I., & Dukes, J. S. (2016). Relationships among land use, soil texture, species richness, and soil carbon in Midwestern tallgrass prairie, CRP and crop lands. *Agriculture Ecosystems and Environment*, 216, 237–246. <https://doi.org/10.1016/j.agee.2015.09.041>
- Yang, J. H., Ji, Z. M., Chen, D. L., Kang, S. C., Fu, C. S., Duan, K. Q., & Shen, M. G. (2018). Improved land use and leaf area index enhances WRF-3DVAR satellite radiance assimilation: A case study focusing on rainfall simulation in the Shule River basin during July 2013. *Advances in Atmospheric Sciences*, 35(6), 628–644. <https://doi.org/10.1007/s00376-017-7120-4>
- Yu, M., Carmichael, G. R., Zhu, T., & Cheng, Y. F. (2012). Sensitivity of predicted pollutant levels to urbanization in China. *Atmospheric Environment*, 60, 544–554. <https://doi.org/10.1016/j.atmosenv.2012.06.075>
- Zhang, H. L., Pu, Z. X., & Zhang, X. B. (2013). Examination of errors in near-surface temperature and wind from WRF numerical simulations in regions of complex terrain. *Weather and Forecasting*, 28(3), 893–914. <https://doi.org/10.1175/waf-d-12-00109.1>
- Zhao, D. M., & Wu, J. (2017). The impact of land use and land cover changes on east Asian summer monsoon precipitation using the WRF-mosaic approach. *Atmospheric Science Letters*, 18(12), 450–457. <https://doi.org/10.1002/asl.788>
- Zhao, P. Z., Li, S., Wang, E. H., Chen, X. W., Deng, J. F., & Zhao, Y. S. (2018). Tillage erosion and its effect on spatial variations of soil organic carbon in the black soil region of China. *Soil and Tillage Research*, 178, 72–81. <https://doi.org/10.1016/j.still.2017.12.022>